Egypt. J. Chem. **Vol. 67**, No. 1 pp. 141 - 156 (2024)

Egyptian Journal of Chemistry

http://ejchem.journals.ekb.eg/

Low cost strontium silicate nanoceramics prepared in water glass medium for bone tissue repair: *in vitro* studies

Hind H. Abdelkader[a], Mostafa Mabrouk[b*], Aida A. Salama[a], and Esmat MA Hamzawy[c],

[a] *Physics Department, Faculty of Science, AL Azhar University (Girls), Cairo, Egypt.*

[b] *Refractories, Ceramics and Building materials Department, National Research Centre (NRC), 33 El Behooth St. Dokki- Giza- Egypt P.O.12622.*

[c] *Glass Research Department, National Research Centre (NRC), 33 El Behooth St. Dokki- Giza- Egypt P.O.12622.*

Abstract

This study aims to develop alternative economic materials for bone tissue repair. Bioactive material was prepared through the nominal composition of strontium silicate $Sr_{0.5}(Ca, Mg)_{0.5}SiO_3$ with partial replacement of $Sr_{0.5}$ with $Ca_{0.5}$ or $Mg_{0.5}$. Differential thermal gravimetery (DTG), X-ray diffraction (XRD), Fourier transform infrared spectroscopy (FT-IR), Transmission electron-microscope (TEM), Scanning electron-microscope (SEM/EDX) and nano-Zetasizer were utilized to evaluate their properties. Moreover, the in vitro assessments such as bioactivity, antimicrobial activities, cell compatibility (cell death mode) and alkaline phosphatase activity (ALP) against MG-63 cell line were also performed. Sr- silicate ($SrSiO_3$), wollastonite ($CaSiO_3$), enstatite ($MgSiO_3$) and cristobalite (SiO_2) were developed through the sintering process at 900 °C/2h. The microstructure shows nanoparticles of the later phases through TEM analysis whereas it accumulated in clusters that indicated by SEM photographs. Also, the zeta potential confirmed that all the nanoceramic particles carry negative charges on their surfaces. The in vitro results of the sintered specimens indicated a great progress in formation of apatite in nano-size scale, through the SEM/EDX microanalysis. However, the antimicrobial properties proved the superiority, of Ca- or Mg-free $SrSiO_3$ sample, against tested microorganisms. Moreover, all nanoceramics demonstrated excellent cell viability. However, the concentrations between 6.25 and 100 µg/ml in the range of (97 to 121) showed the highest viability percentages. These findings supported the beneficial effects of Si and transition metals (strontium, calcium, and magnesium) on cell survival. In addition, ALP results confirmed a good cells differentiation, which obviously revealed in SrCS sample. These results suggested that silicate ceramics prepared in this study and doped with selected transition metals are applicable to regenerate bone tissue.

Keywords: Sr- silicate; water glass; bioactivity; antibacterial; cell death mode

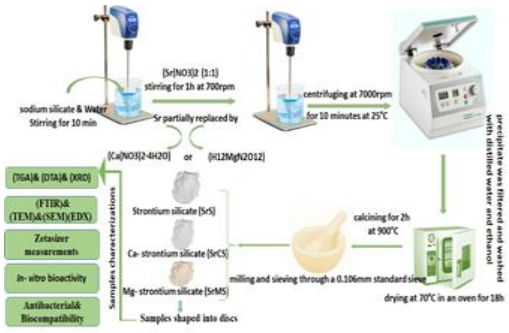

Graphical abstract

1. Introduction

The repair process of bone for skeletal problems generated by congenital bone diseases, infectious diseases or accidents is one of the major challenges for clinical surgery **[1].** The most applicable approaches for bone grafting, are autograft and allograft known as "gold standard method" **[2].** However, they have some draw backs that cause limitation of their use such as limited availability, lack of suitable grafting source, and lengthened waiting for surgery to take place, which may arise in surgical risks and complication for the patients **[3].** Gold standard method isn't the only method to restore bone defects, but there is some other route for treatment, such as orally anti osteoporotic drugs include strontium ranelate which has proven effective in reduction of the occurrence of

*Corresponding author e-mail: mostafamabrouk.nrc@gmail.com

Receive Date: 11 April 2023, Revise Date: 11 June 2023, Accept Date: 20 June 2023

DOI: 10.21608/ejchem.2023.205524.7859

fractures in osteoporotic patients. This takes place through strontium, which is one of the most important elements and necessary for bone reformation and its general health. Particularly, it is deposited in human teeth and bones in a significant proportion up to 99.1% of Strontium absorbed in to the human body **[4,5].** Therefore, Sr is accountable for the regulation of bone metabolism process, it works on bone resorption through inhibiting the activity of osteoclast and simultaneously stimulate osteoblasts know as dual regulation effect. It also has a role in the process of calcium deposition in bone, which is why Sr is important for bone construction and regeneration **[6].**

Although Strontium ranelate contains an organic moiety as well as ranelate carries two atoms of strontium **[7]**, but unfortunately some side effects of this drug were found which made its use restrictive and strict including a rise in the incidence of cardiovascular diseases **[8]**. To overcome these problems, researchers were motivated to develop synthetic biomaterials; in particular strontium containing biomaterials received extensive attention by researchers to be utilized for application in the field of bone reconstruction. Among these materials, nanoceramic materials which might be prepared by various methods, such as microwave treatment **[9]**, hydrothermal **[10]** and hydrolysis of alkoxides (sol-gel) **[11]**. However, these methods face few difficulties including complicated handling conditions and expensive starting materials. These factors may not offer the potential needs for such materials that are used in different fields, this impedes its widespread production **[12].** On the contrary, wet precipitation method which has a lot of advantages including controlling the pH of solution or the reactants and the solvent type, in addition to that, low cost starting materials are applicable. The common low cost materials used in preparation of nanoceramics is commercial sodium silicate as source of silica **[13,14].**

Silica is known to be a tetravalent metallic element located in group 14 of the periodic table; it's also considered an essential element of the human body **[15].** Silica is one of the most abundant elements found in the earth's crust and it occur as different oxides and silicates because of its high chemical affinity with O_2 element, thus it is a vital essential element of biological processes, such as regulation of bone metabolism, silica mainly affects the quality of newly constructed bone **[16,17].** Additionally, incorporation of transition metals such as strontium Sr, magnesium Mg, calcium Ca to the ceramic materials have given a progression of structural, physical, mechanical and biocompatibility properties, for example, degradation, restoration, and bone healing capacity **[18].** Moreover, several studies have suggested silicate bioceramics containing transition metals enhance bone reconstruction, which mainly because of the release of silicon and transition metals ions that promote the adhesion and proliferation of osteoblast cells **[19,20].** Khan et al **[1]**, found that single and binary doping of strontium and lithium in bioactive glass promote excellent osseous tissue formation. Mei et al **[21]**, have designed calcium silicate (CS) bioceramic discs with flower-like nanostructured surfaces for bone regeneration, which were subjected to in vitro tests. The outcomes revealed that these materials, compared to CS bioceramics with flat surfaces, greatly enhanced osteogenic differentiation and bone repair by promoting cell adhesion and proliferation. Alecu et al **[22]**, have developed porous ceramics based on forsterite (Mg_2SiO_4) for bone tissue regeneration by incorporating a porogenic agent and varying heat treatments. When the samples' in vitro cytotoxicity was examined, the sample sintered at a higher temperature had somewhat greater cell viability and seemed to encourage easier surface adhesion. Abo-Mosallam and Mahdy **[23]**, have enhanced thermal and mechanical properties of glass ceramic material by doping with both MgO and SrO.

Accordingly, the main aim of this research is to design strontium silicate ($SrSiO_3$) by the wet method in a water-glass solution, with partial replacement of Sr with Ca^{2+} or Mg^{2+}. The prepared samples were characterized using TGA, DTA, XRD, SEM/EDX, TEM, FTIR, and Zeta-Potential. Bioactivity was tested *in vitro*. Also, the antibacterial activity against gram-negative and gram-positive bacteria was investigated for the samples. Finally, the biocompatibility of the obtained nanoceramics against the MG-63 cell line was also investigated.

2. Materials and methods

2.1 Materials

The strontium silicate $SrSiO_3$ was prepared through the wet method in water-glass medium with partial replacements of CaO/SrO and MgO/SrO. Water glass [$Na_2O(SiO_2)$ x · xH_2O] containing about 38 g of sodium oxide (Na_2O) and 62 g of silicon dioxide (SiO_2) per liter. The water glass was mixed with calcium oxide (CaO), magnesium oxide (MgO) and strontium oxide (SrO) precursor salts in order to obtain low cost nanoceramics. The sources of the later oxides were calcium nitrate tetrahydrate (Ca (NO3)2.4H2O, 236.10 g/mol, Alpha, India), magnesium nitrate hexahydrate (Mg (NO3)2·6H2O, Mw=256.41 g/mol, Merch, Germany) and strontium nitrate (Sr (NO3)2, Mw=211.63 g/mol, Sigma Aldrich, India).

2.2 Preparation of nanoceramics

The fabricated nanoceramics were coded as SrS, SrCS and SrMS as demonstrated in **Table 1**. They were synthesized by a wet-chemical precipitation method **[24,25].** In particularly, SrS sample was obtained by dissolving of sodium silicate in appropriate amount of distilled water under stirring at 500 rpm for 10 minutes. Subsequently, strontium nitrate was dissolved into sodium silicate solution with molar equivalent amount under continuous stirring for 1 h at 700 rpm. The pH values of reactant solution were adjusted to 9 by adding acetic acid. The mixture was centrifuged for 10 minutes at 7000 rpm. for filtration and washed several times by distilled water and ethanol to remove impurities. Afterwards, the collected precipitates were dried in an oven at 70^{o}C for 12h and then calcined at 900^{o}C for 2h. Finally, calcined samples milled into powder and sieved from a 0.106 µm standard-sieve to shape into discs with specific height and diameter by using stainless-steel die under a pressure of 10 ton. SrCS sample was obtained by replacing 50 wt% of strontium in SrS by calcium, and SrMS sample was obtained by replacing 50 wt % of strontium SrS by magnesium as shown in the Table 1.

2.3 Nanoceramics Characterizations

Differential thermogravimetric analysis (DTG, UniversalV4.5A TA Instruments, New Castle, DE, USA) was used for the dried specimens (at 70 °C) to show the weight loss and crystallization temperatures. The heating temperature in the DTG was raised to 1000 °C with heating rate set to 10 °C/min. Calcined samples were subjected to the X-ray diffraction analysis to identify any crystallization in the samples. The x-ray diffraction analysis was evaluated using (XRD, Axs D8 ADVANCE, Bruker, Karlsruhe, Germany) and the pattern was measured at 2Ɵ between 10°–70° and applied current 40 mA at 40 kV of voltage.

To identify the structure and functional group of calcined samples the Infrared spectroscopy analysis (FTIR) was performed. The FTIR spectra were performed at room temperature with scanning from 400 -4000 cm^{-1} using (FT/IR-4600 type A, Jasco, minzencity, Germany) with a resolution of 8 cm^{-1}. The charge and size distribution of calcined powder samples were determined using Dynamic- light scattering [DLS] (Zetasizer - Nano ZS, Malvern Instruments, UK). Transmission electron microscopy (TEMJEM2100, JEOL, Japan) was used to show the morphology of the powder of the calcined samples. Also, the scanning electron microscopy (SEM/EDX, JEOL JXA-840A, Japan) attached with energy dispersive x-ray microanalysis was used to confirm the morphology and the chemical analysis of the calcined powder.

2.4 Bioactivity of nanoceramic

To perform the *in vitro* bioactivity test, ceramics nanopowders were shaped into discs with specific height and diameter (0.5x1.0 cm) by using stainless-steel die under a pressure of 10 ton. Individual discs were soaked in 60 ml of simulated body fluid (SBF) at 7.4 pH in plastic measuring containers, these containers were put in incubator at 37^{o}C for 2 weeks. After the 2 weeks, the discs were washed by distilled water and ethanol to stop the reaction. Then, discs were dried at 37^{o}C for overnight to be ready for characterization by FTIR and SEM coupled with EDX.

2.5 **In vitro antimicrobial activities**

2.5.1 **Microorganisms**

In vitro antimicrobial activity was examined for suspended nanoceramics in phosphate buffer solution (PBS). The bacteria utilized in this study were gram-positive bacterial strains (Staphylococcus aureus ATCC-6538), gram-negative bacterial strains (Escherichia coli ATCC-25922), and fungi (Candida albicans ATCC-10231).

Sample code	Samples formula	weight	Chemical compositions				
		wt.%	Na_2O	SiO_2	SrO	CaO	MgO
SrS	$SrSiO_3$	weight	7.60	12.40	20.71		
		wt.%	18.67	30.46	50.87		
SrCS	$Sr_{0.5}\ Ca_{0\cdot5}SiO_3$	weight	7.60	12.40	10.36	5.59	
		wt.%	21.14	34.49	28.82	15.55	
SrMS	$Sr_{0\cdot5}\ Mg_{0\cdot5}SiO_3$	weight	7.60	12.40	10.36	_	4.02
		wt.%	22.1	36.07	30.13	_	11.70

Table 1 Chemical composition of the batches in grams and weight %

These microorganisms were from the American Type Culture Collection (ATCC, Rockville MD, USA), and Northern Utilization Research and Development Division, Department of Agriculture, Peoria, Illinois, USA (NRRL). The bacterial strains were sub cultured in fresh nutrient agar (NA) medium (Merck, Darmstadt, Germany) for 24h before the test. The fungi were cultivated for seven days at 28 °C on potato dextrose agar media (PDA) (Lab M., Bury, Lancashire, UK) before running the experiment.

2.5.2 Antibacterial test of nanoceramic

The agar well diffusion method reported by Jorgensen and Turnidge was used to create the antibacterial screening bioassay **[26]** using Mueller-Hinton agar (Lab M Limited, Bury, Lancashire, UK), then the plates allowed to diffuse for 2 h at 4°C. The experiment was assessed in triplicate, and all of the plates were incubated for 48h at 28 to 30°C for the fungal strain and 24h at 37°C for the bacterial strain. The wells' clearance zones were observed and gauged in milli meters [**27**]. Standard antibiotics streptomycin (10µg), ampicillin (30µg) and Clotrimazole (50µg) were used as positive drug control.

2.6 Cytocompatibility of Nano ceramic.

2.6.1 MTT Cytotoxicity

The MTT (3-[4,5-dimethylthiazole-2-yl]-2,5-diphenyltetrazolium bromide), acquired from (Merck KGaA (Darmstadt, Germany)). It is utilized to evaluate the cytotoxicity of the tested specimens on human osteosarcoma (MG-63 cell line). It relies on the ability of active mitochondrial dehydrogenase enzyme in living cells being able to incision the yellow MTT's tetrazolium rings and create dark blue insoluble formazan (crystals) directly proportional to the number of viable cells. In particular, cells ($1x10^4$ cells/well) were cultured in the DMEM medium in a flat bottom (96-well microplate) and addressed with (20µl of serial dilutions of the tested samples) starting with 200µg/ml and ending with 6.25µg/ml. The test was conducted over 24h at 37ºC in a humidified 5% CO_2 atmosphere. The media were removed once the incubation period had ended and (40µl MTT solution/well) were added and incubated for an additional 4h. The MTT crystals were dissolved by adding 180µl of acidified isopropanol per well, and the plates were then shacked at room temperature. The absorbance at 570nm was then determined photometrically by a microplate ELISA reader. (FLUOstar OPTIMA, BMG LABTECH GmbH, (Ortenberg, Germany)). Trice repeats were carried out for each concentration, after that the average was calculated.

2.6.2 Cytotoxicity test via fluorescence microscope

The cell death mode of the prepared samples SrS, SrCS, and SrMS at concentrations of 214.7, 241.5, and 234.4g/ml, respectively, was evaluated against MG-63 cells at a density of 10^4 cells per well. Where the cells were plated on eight-well cell culture slides (SPL, Seoul, South Korea). Each slide was stained with acridine orange and ethidium bromide following the incubation time (24h) (AO/EB:100µg/ml in certain volume of PBS), all obtained from (Merck KGaA (Darmstadt, Germany)). Then, to determine the mode of cell death, the stained cells were seen using a fluorescence microscope (AxioImager Z2, Zeiss, Jena, Germany). Cells with green color were recorded as viable cells, while the cells with yellow,

orange, or red colors account for early apoptotic, late apoptotic or necrotic cells, respectively. Images were taken by a digital camera (Axio Cam MRC3 (S/N 4299)). For each sample, the experiment was carried out three separate times.

2.7 Alkaline phosphatase activity

To examine the effect of the designed specimens on the differentiation of the controlled cells, the ALP activity was performed through the Alkaline Phosphatase Assay Kit ((Fluorometric) (ab83371) (Abcam, Waltham, MA, USA)). Depending on the manufacturer's protocol, the supernatant of the cells after treatment with at concentration of 100µg/ml of each sample versus the untreated control cells. The examination is relied on the capability of ALP to incision the phosphate group of the (non-fluorescent 4-Methylumbelliferyl phosphate disodium salt) (MUP) substrate, when the substrate is dephosphorylated, increases fluorescent signal (Ex/Em= 360 nm and440 nm). It was examined by microplate reader FLUOstar OPTIMA (BMG LABTECH GmbH, (Ortenberg/ Germany)).

2.8 Statistical analysis

In this study, all data were reported as mean ± standard error of mean. One-way ANOVA and the Dunnett post hoc test were used to evaluate statistical significance.

3. Results and discussion

3.1 TGA and DTA

The thermal behavior of materials depends on two important factors, the composition and the preparation method of the nanoceramics **[28].** The thermogram of the prepared sample powders SrS ($SrSiO_3$), SrCS ($Ca_{0.5}Sr_{0.5}SiO_3$) and SrMS ($Mg_{0.5}Sr_{0.5}SiO_3$), after dryness (70 °C/24h) are indicated in **Figure 1**. Due to the formation of some compounds during the preparation process, the heat decomposes the formed hydrated, hydroxynated and the residual carbonates compound.

In TGA curves, the weight reduction of the dried samples up to 1000 °C were about 21.94%, 47.09% and 36.29% for SrS, SrCS and SrMS samples, respectively. In the DTA curves the exothermic peaks were between 800-900ºC which centered at 860 ,850 and 873ºC, for SrS, SrCS and SrMS samples, respectively referred to crystallization temperature. In SrS sample small broad hump was observed at 860 °C while the partial replacement of SrO by CaO in SrCS led to the appearance of a more broad peak at 850°C.

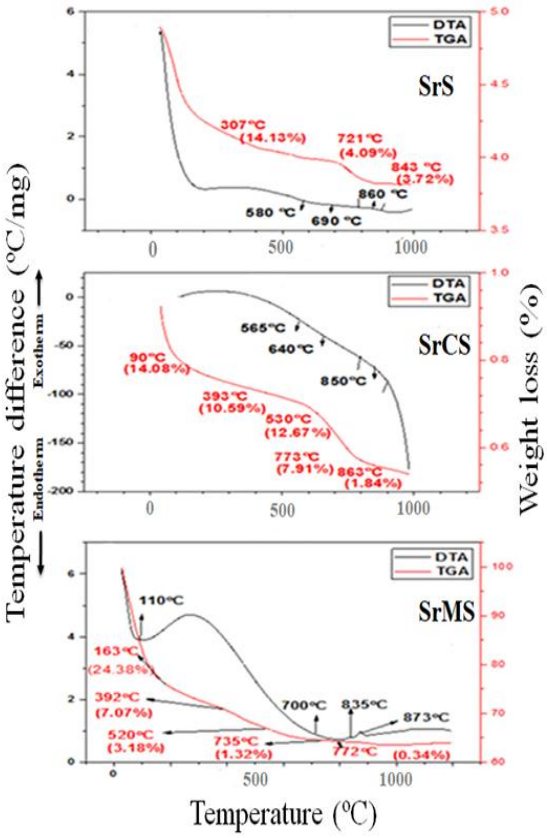

Figure 1 TGA and DTA of dried SrS, SrCS and SrMS samples.

Also, the partial replacement of SrO by MgO in SrMS sample form a clear small peak at 873°C (**Figure 1**). Therefore, the dried powders were sintered at the selected temperature (900 ºC). The increase in weight reduction for both SrCS and SrMS samples possibly because structural water, since most of the weight reduction was at first and second stages (at 90, 393ºC and 163, 392ºC for both SrCS and SrMS ceramics, respectively) **[29, 30]**. In addition, the increase in weight reduction of SrCS sample possibly because presence of Ca ions that's results in high Ca:Si ratio that cause more weight reduction [**31**]. For the SrS sample, the first stage, ranging from room temperature to 307.61ºC and represent about 14.13% from weight reduction. The weight reduction was caused by elimination of free water that have not been removed during the drying process as well as probably partial removal of some nitrates. While, the next stage of the weight reduction at 721ºC was around 4.09% which can be

ascribed to remove of residue nitrates, where all the nitrates were completely eliminated at 560ºC and maybe referred to de carbonation at low-temperature [**32**]. Finally, The third stage of weight reduction may be attributed to de carbonation at high-temperature [**33]**. However, it is suggested that de carbonation is incomplete according to a previous study, where the heat treatment at 900 ºC leaves carbonate residue in the sample [**34**].

3.2 XRD analysis

Identification of the developed phases after dryness and sintering the specimens at 900 °C are shown in **Figure 2**. The XRD pattern of the sintered specimens show the formation more than one phase include silicate of strontium, calcium, magnesium and silica as well. In the SrS sample crystallization of $SrSiO_3$ (ICDD - # 96-200-6167- orthorhombic- its ratio ~ 76.1%) and cristobalite (ICDD - # 96-101-0939- tetragonal- its ratio ~ 23.9%) were identified. It is proposed that $SrSiO_3$ phase formed as a result of the combination of equivalent amount of cristobalite (SiO_2) with strontium oxide (SrO) during crystallization process **[35].** In case of partial CaO/SrO replacement led to the appearance of three phases including wollastonite (ICDD - # 96-900-5779- monoclinic- its ratio ~ 61.6%), $SrSiO_3$ and cristobalite (**Figure 2).** Despite the chemical similarity between Sr and Ca, the difference in the ionic radius for both of them may lead to decrease the crystallization degree as compared to native sample (SrS), this may possibly be ascribed to occurrence of the ceramic matrix expansion. Also, partial replacement of Mg instead of Sr led to the appearance of three phases including magnesium silicate (enstatite) (ICDD - # 96-901-4118- orthorhombic - its ratio ~ 69.9%), $SrSiO_3$ (ICDD - # 96-200-6167- orthorhombic- its ratio ~ 22%) and cristobalite (ICDD - # 96-101-0939- tetragonal- its ratio ~ 8%). It is essential to note that magnesium may be housed in network structure as network former (MgO_4) or modifier (MgO_6), based on the percent of alkali in the material composition **[36, 37].** This indicates that the major amount of Mg enters as network modifier in the material structure which results in orthorhombic magnesium silicate Mg (SiO_3). The presence of sodium provided by the water glass medium encourages the formation of the cristobalite and strontium silicate in all the nanoceramics, which stress out its importance in preserving these main phases.

3.3 FTIR

The FTIR spectra of the prepared samples calcined at 900 °C/2h was depicted in the Figure 3. The SrS sample shows bands located at 1619 and 1635.34 cm-1 which refer to OH bending vibration, while the broad band at 3430.74 cm-1 corresponding to OH stretching vibration of water absorbed from atmospheric moisture [12]. Also, the narrow band was observed at 1384 cm-1 which may be correspond to carbonate group which may result from interaction between prepared materials and atmospheric CO2 during sintering process [38,39]. Furthermore, other bands recorded at lower wavenumber between 400 cm-1 and 713 cm-1 indicated the presence of the Si-O-Si bending vibration in (SiO44-) silicate tetrahedron and the band at 713 cm-1 are attributed to Si–O symmetric stretching in silicate group [40,41]. On the other side, partial CaO, MgO/SrO replacement revealed nearly similar appearance as in the SrS sample with slight shift of bands that at 489 and 649 cm-1 shifted into 495 and 678 cm-1 in SrCS sample while in the SrMS sample the bands shifted to 493 and 651 cm-1. Also, the band located at 970 cm-1 referred to Si-O-Si in SrCS and SrMS samples which was absent in SrS sample [38]. It is clear that the band at 1384 cm-1 has become very broad and also the intensity of OH band at around 3415 and 3411 cm-1 in case of SrCs and SrMS with comparison with SrS sample. The later variations maybe due to the crystallization of wollastonite in SrCS and enstatite in SrMS sample.

However, appearance of 420 and 472 cm-1 bands in the SrMS sample indicate that Mg 2+ ions can be occupied octahedral coordination in crystal lattice [42].

3.4 TEM analysis

TEM photographs of SrS, SrCS and SrMS powder samples calcined at 900° C/2h are shown in Figure 4. All the samples demonstrated irregular particles in nano-size scale between 7 and 81 nm. The formed ceramic particles were from 7 to 22 nm in SrS sample, from 33 to 81 nm in SrCS and from 5 to 8 nm in SrMS sample. It is clear that the replacement of CaO/SrO led to increase the particles size, while MgO/SrO replacement led to decrease the particles size.

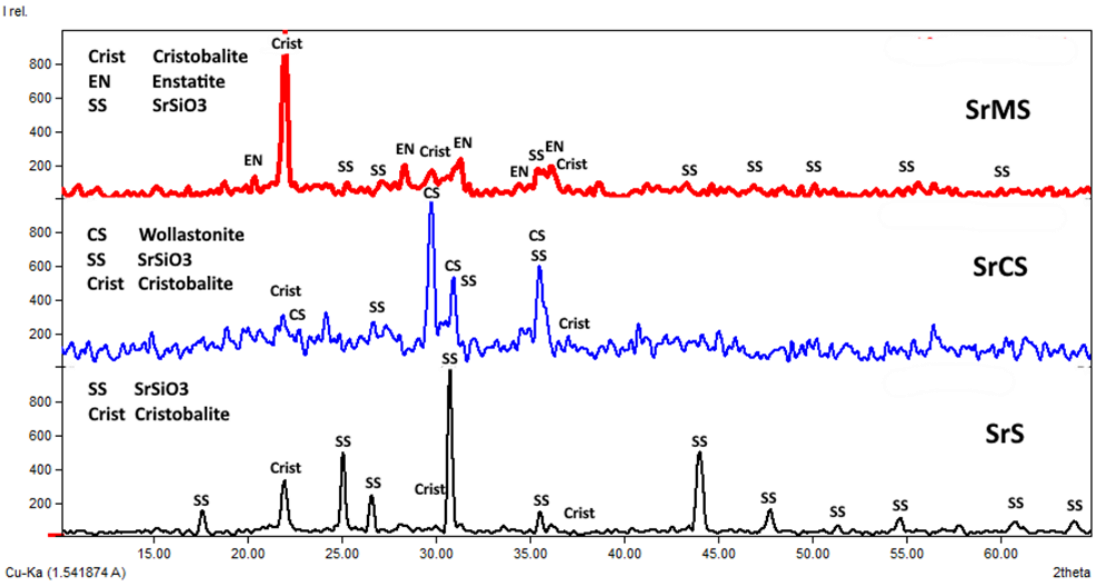

Figure 2 X-ray diffraction patterns of the nanoceramics sintered at 900 °C/2h.

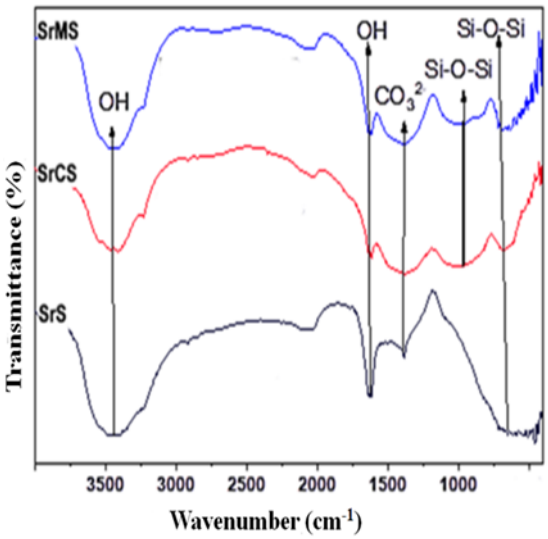

Figure 3 FTIR Spectra of SrS, SrCS and SrMS samples sintered at 900°C/2h**.**

The increase in particle size in SrCS may result from unit cell volume expansion caused by the difference in atom diameter between Ca^{2+} and Sr^{2+}, where the ionic radius of both calcium and strontium are 1.13 Å and 1.00 Å, respectively, thereby increasing size could be attributed to larger ionic radius of strontium **[43]**. Moreover, the reduction in the particles size of SrMS sample as compared to native ceramic could be ascribed to the Mg^{2+} that acts as modifier in crystal network and increases the crosslinking of network, therefore, leads to reduction of size and increase the field strength [**23**]. The previous studies confirmed that bioceramic present in nano to sub micro-scale possess a good cells adhesion, proliferation and bone formation because of the large surface area provided by nanoparticles **[44].** On the other hand, selective/area electron diffraction (SAED) pattern of all samples demonstrate extensively crystallization. Particularly, SrS sample revealed incomplete rings which indicate that the sample maybe in an intermediate material stage that the diffraction is from single and polycrystalline substance. While, SrCS sample showed randomly distributed spots appear in semi-circular paths that may be point to decline in the crystallization of the sample owing to Sr^{2+} of partial substituted by Ca^{2}. Furthermore, SrMS sample indicated two parallel planes with different kind of spots include big and bright spots and also small and dim spots, due to that it is suggested that the sample contains more than one phase. It should also be noted that the appearance of parallel lines with spots are evidence of crystal perfection [**28].**

3.5 SEM with EDX analysis

The SEM micrographs of the present SrS, SrCS and SrMS samples after sintering at 900ºC for two hours are shown in Figure 5. The micrographs images of samples revealed irregular and rough surfaces consisting of agglomerated particles with different morphologies and voids between them. The later agglomeration of the particles may be caused by the sintering process. The microstructure of SrS sample revealed interconnected-agglomerate particles with low formation of gaps. In the substitution of

CaO/SrO in SrCS sample, the microstructure became more porous in sub-spherical structure while in the SrMS sample was fairly uniform with denser microstructure of sample (Figure 5).

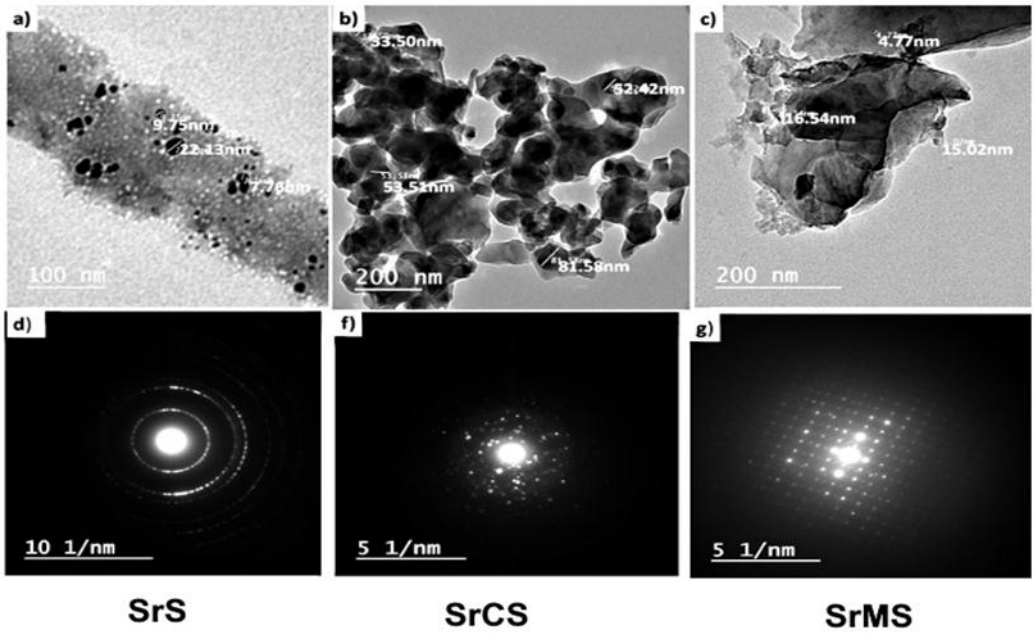

Figure 4 TEM photographs and SAED of a,d) SrS, b,f) SrCS and c,g) SrMS sintered powder samples at 900 °C/2h.

It should be noted that the samples possess a variable particles diameter, where the particles diameters for prepared samples sizes range from nano to sub-micro, the particle diameter for SrS sample ranging from 99 to 192 nm. While, SrCS sample appeared with particle diameter in range of 315-463 nm. Furthermore, SrMS sample exhibited a particle diameter of 141-287 nm. It is observed that the SEM results are slightly different from TEM results owed to that the SEM technique is based on visual observation of sample in bulk state, where the TEM results are based on dispersed particles in solution, therefore, the particles were in agglomeration in the case of SEM and were nanoparticles in case of TEM. The EDX microanalyses of the sintered specimens at 900°C/2 h are shown in the **Table2.** The EDX analysis revealed the presence of essential elements of the developed phases in SrS, SrCS and SrMS, i.e. $SrSiO_3$, $CaSiO_3$ and $MgSiO_3$ (**Table 2**).

3.6 Zetasizer measurements

Zeta potentials of nanoparticles were carried out to evaluate the stability of particles. From **Figure 6**, zeta potentials values for the samples SrS and SrMS are observed at -23.4 and -24.5 mV, respectively, while SrCS was at -18.6 mV. The later values indicate that zeta potential values of all samples in suspended system were negative and in convergent range. According to previous studies, the particles could be said to be stable if the potential values in range of +30 to -30 mV [**45**]. With increased repulsive forces between the crystalline particles that are dispersed in a suspended media, where repulsive forces between the particles are caused by higher surface charge (negative charge), the stability of the particles increases [**46**]. The repulsive forces mean that the particles repel each other, which in turn preclude aggregation and achieve stability for the samples [**47**].

Figure6 (d, e and f) indicate the hydrodynamic diameter of the prepared samples through particle size distribution measurement by intensity. The average size value was 181.5 nm for SrS sample while substitution of Sr^{2+} by Ca^{2+} or Mg^{2+} resulted in an increase in the average size value to 184.3 nm for SrCS sample and reduced to 137.5 nm it for SrMS sample. The increase in diameter for SrCS sample could be explain based on the difference in atom diameter, in addition to unit cell volume expansion result of replacement. While, the reduction in

diameter for SrMS sample it is suggested that it results from decrease in spacing in the crystal structure because of the partial substitute of SrO by MgO [**23,48**]. It must be mentioned that the result of zetasizer determination of particles size results may therefore be slightly different from TEM and SEM.

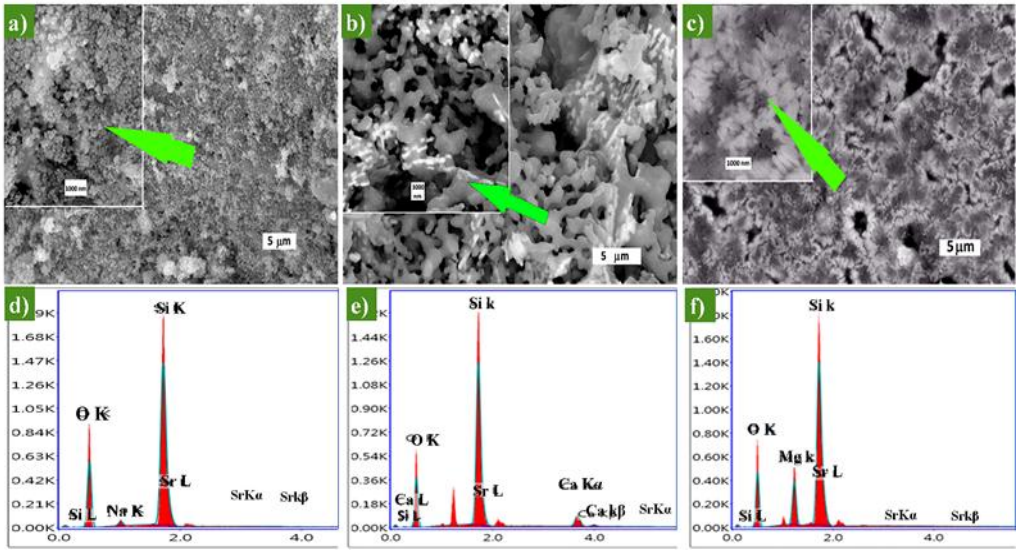

Figure 5 SEM and EDX of a, d) SrS, b, e) SrCS and c, f) SrMS samples sintered at 900 °C/2h.

Table 2 EDX microanalysis of SrS, SrCS and SrMS samples sintered at 900 °C/2h.

	EDX microanalysis						
	Formula	O	Si	Sr	Ca	Mg	Na
SrS		49.70	34.57	12.96	---	---	2.77
Nominal	$SrSiO_3$	29.32	17.16	53.62	----	----	----
SrCS		47.11	35.57	11.77	5.55	---	Nd
Nominal	$Ca_{0.5}Sr_{0.5}$ SiO_3	34.31	20.08	31.31	14.31		
Nominal Wollastonite	$CaSiO_3$	34.50	24.18	----	41.32	----	----
SrMS		40.72	31.35	17.95	---	9.98	Nd
Nominal	$Mg_{0.5}Sr_{0.5}SiO_3$	36.35	21.27	33.17		9.21	
Nominal Enstatite	$MgSiO_3$	47.81	27.98	----	----	24.21	----

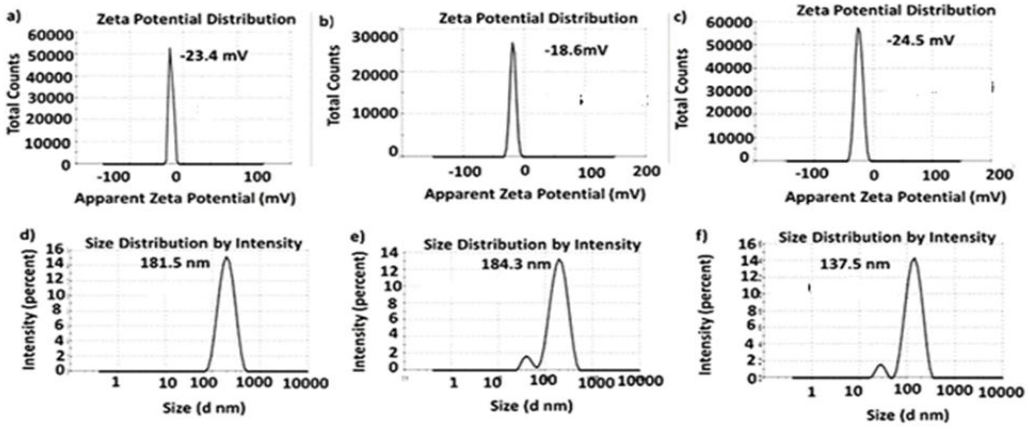

Figure 6 zeta potential and particlesize distribution of a,d) SrS, b,e) SrCS and c,f) SrMS powder samples heat-treatd at 900 °C/2h.

3.7 Bioactivity of nanoceramic analysis

The bioactivity of the SrS, SrCS and SrMS samples sintered at 900 °C/2h were examined by FTIR and SEM coupled with EDX after soaking in SBF for 15 days. Primarily, FTIR spectra of all samples after soaking in SBF reveals the presence of carbonate and phosphate functional groups in addition silicate group as shown in Figure 7. FTIR spectra of $SrSiO_3$ revealed two new bands at 553 and 620 cm^{-1}, which are referred to P–O bending in PO_4^{3-} group. Furthermore, the double bands are observed at 927 and 972 cm^{-1} that can be pointed to stretching vibration of C–O in carbonate group [49,50], confirming the formation of carbonated apatite layer on $SrSiO_3$ surface. Moreover, the bands at 706, 795, and 1075 cm^{-1} corresponded to silicate group assuring the presences of Si- rich layer, which forms before apatite phase [51,52]. While, the FTIR spectra of SrCS sample revealed two new bands at 965 and 637 cm^{-1}, which may be referred to PO_4^{3-} group. Other bands are observed at 870 and 1406 cm^{-1} corresponded to CO_3^{2-} group as well as the bands at 468, 794, and 1078 cm^{-1} pointed to silicate group [49-51]. FTIR spectra of SrMS sample revealed the phosphate bands at 554 and 733 cm^{-1}, while the carbonate bands observed at 859 and 896 cm^{-1}, also the bands that related to silicate group revealed at 467, 1010, 1075 cm^{-1} [49-52]. The SEM micrographs coupled with EDX microanalysis for the surfaces of the pre-sintered samples and after soaking in SBF for 15 days were indicated in Figure 8. The SEM photographs showed new crystalline film of apatite layer deposited on the surfaces of the samples. The photograph of SrS sample revealed different size of irregular clusters of tiny particles in nano-size scale of apatite. The photographs of SrCS and SrMS samples show accumulated clusters of well sorted rounded nano-size apatite (Figure 8). The EDX spectrum showed the precipitation Ca and P in all the samples that confirm the formation of bioactive apatite layer on SrS, SrCS and SrMS surfaces **(Figure 8).**

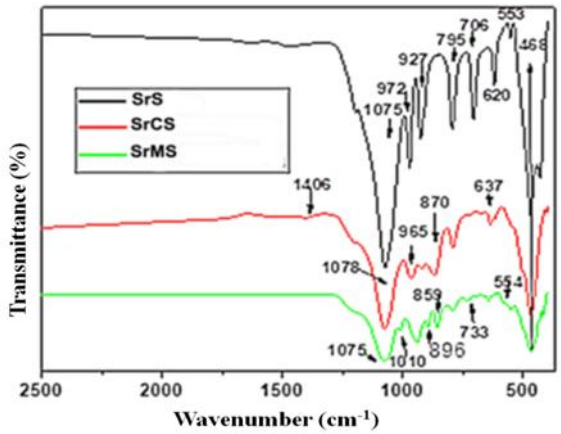

Figure 7 FTIR spectra of the SrS, SrCS and SrMS samples sintered at 900 °C/2h.

The Ca/P ratios were 0.622, 4.75and 0.38 for SrS, SrCS and SrMS samples, respectively. The obtained ratios are not following the traditional apatite, which could be owed to the fact that the presence of Sr (1.13 Å) which can substitute Ca (1.00Å) and adjust the formation apatite. However, the composition of apatite-group may be containing high Na or transition metals such as Sr and Mg or rear earth elements (REE) that result in changes in the ratios of Ca and P in the formed apatite as the following compositional range: (Ca0.34–4.49Sr0.18–4.54Na0.05–0.30REE0.08–0.18Ba0–0.10)(P2.87–3.03Si0–0.16)O12(F,OH) [43,53].

3.8 Antibacterial test of nanoceramic

Figure 9 indicates the antimicrobial activity of the present sintered materials against three microbes by using the agar diffusion method. The outcomes (inhibition zone (IZ) in mm) were represented in the Table 3. It is interesting that the majority of the samples examined in this study exhibit a fair level of antibacterial activity against the majority of the pathogens that were tested. In the case of (G+) bacteria: Staphylococcus aureus, both of SrS and SrCS samples confirmed a moderate inhibitory activity with IZ 12 and 15mm, respectively whereas. While the SrMS sample showed no inhibitory impact on the investigated microorganisms. In the other (G-) bacteria (E. coli), the inhibition of E.coli growth was observed for SrS with IZ of 15mm. The other two nanoceramics showed no inhibitory impact in examination with the antibacterial standard. In general, the release of alkaline ions especially Ca^{2+} ions promote antimicrobial activity through increasing of the (pH) of the medium and consequent adequate to inhibit the bacterial growth but in our study, antimicrobial activity was showed for sample that contain calcium toward *Staphylococcus aureus* only **[54].** This result may because of the difference in bacterial cell walls of different strains, since Escherichia coli possess an outer membrane with lipopolysaccharides as well as a thin layer of

peptidoglycan, thus, it has a far more complex system compared to Staphylococcus aureus that have thick layers of peptidoglycan only.

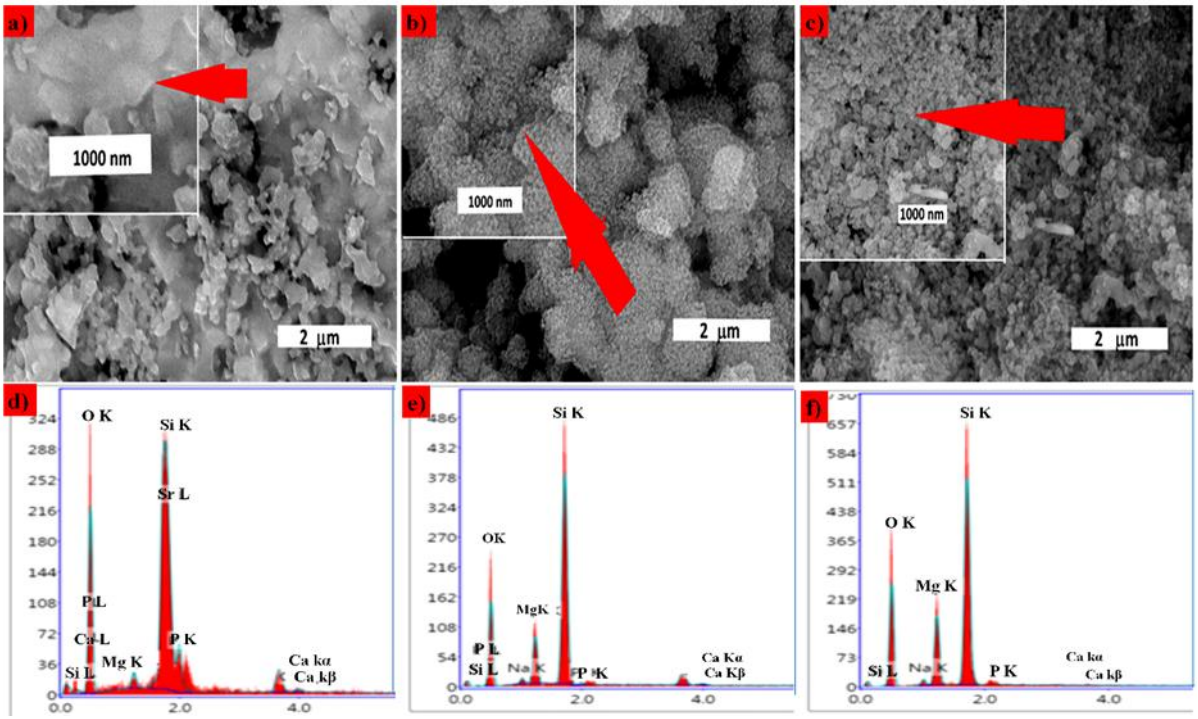

Figure 8 SEM and EDX of a,b) SrS, b,e) SrCS and c,f) SrMS samples after being soaked in SBF for 15 days.

This complex system of Escherichia coli may induce more resistance to antibacterial agent penetration, which could explain why nanoceramic containing Ca^{2+} lacks the antibacterial activity toward Escherichia coli **[55].** It was observed that the SrMS sample that contains magnesium possesses no inhibition zone with respect to both Staphylococcus aureus and Escherichia coli, and its negative effect on the antibacterial activity could be attributed to catalase that is excreted by bacteria (Staphylococcus aureus), which acts on the neutralization of hydrogen peroxide to water (H_2O) and oxygen (O_2) **[56].** Whereas, the mechanism of inhibition of bacterial growth in the SrMS sample can depend on hydrogen peroxide production as an oxidizing agent that has the ability to attack and damage the bacterial cell wall and consequently cause the death of bacteria. It can also be argued that Mg-containing materials lack antibacterial activity because Mg ions are not toxic and thus have no effect on inhibiting bacterial growth, as mentioned in the previous study **[56, 57].** While, in the case of Candida albicans (Yeast) all the prepared samples showed moderate inhibition effects with IZ ranged from 12-15mm in contrast to the utilized antifungal standard.

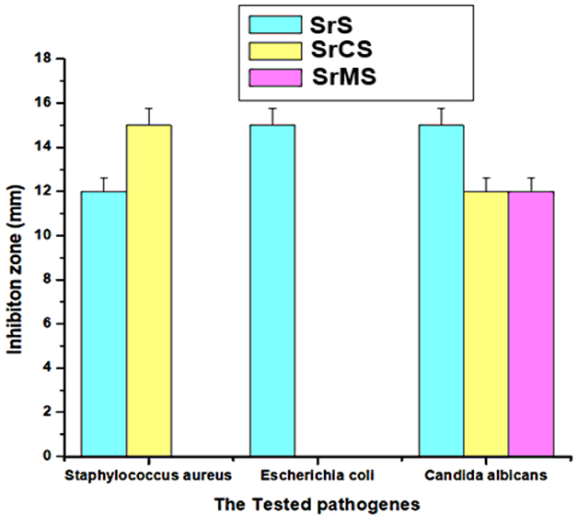

Figure 9 The bacterial inhibition zones of the sintered samples**.**

3.9 Cytocompatibility of nanoceramics

To examine the potential of nanoceramics samples to be utilized in bone tissue engineering, the cell viability by using the MTT assay in addition to the mode of cell death were performed against MG-63 cells for 24h. **Figure 10** demonstrated that all nanoceramics revealed good cell

viabilities. However, the highest viability percentages were observed at concentration ranging from 6.25-100µg/ml within range of (97-121). These outcomes confirmed the positive effect of Si as well as transition metals (Sr, Ca, Mg) on the cell viability **[58, 59].** On the other hand, the present samples revealed little cytotoxicity at higher concentrations as showed in **Figure 10**. This was also supported with the mode of cell death assay via fluorescence microscope, which was performed at concentration of IC_{50} as shown in **Figure 11.** It is worthy to highlight that the mode of the most of nonviable cells was apoptosis cell death type. In details, the mode of cell death for SrS sample indicated early and late apoptosis with slight necrotic records, while SrCS sample revealed only early and late apoptosis nonviable cells, also SrMS sample showed only early apoptosis. It is well known that apoptotic mode of death is not caused by the cytotoxicity of the tested samples but teaks place through the phagocytosis effect that tack place when the cell multiplication rate is fast for example [**60**]. Moreover, the distribution of cell death modes (**Figure 12**) was evaluated from the obtained fluorescent images in (**Figure 10**), where the green color represents the vital cells, while orange, or red colors represent early apoptotic, late apoptotic or necrotic cells, respectively. These results illustrate that nanoceramics can be safely utilized for bone tissue applications as biocompatible substances, especially at concentration of (6.25 to 100µg/ml) .

Sample code	IZ (mm)		
	G-Positive bacteria *Staphylococcus aureus* ATCC-6538	G-Negative bacteria *Escherichia coli* ATCC-25922	Fungi *Candida albicans* ATCC-10231
$SrSiO_3$	12.0	15.0	15.0
$Ca0.5Sr0.5SiO_3$	15.0	0.0	12.0
$Mg0.5Sr0.5SiO_3$	0.0	0.0	12.0
A*	20.0	17.0	0.0
B*	20.0	20.0	0.0
C*	0.0	0.0	30.0

Table 3 The compounds' antimicrobial activity was assessed using the agar diffusion method Antibacterial Standard; A = Streptomycin (10 µg); B = ampicillin (30 µg); Antifungal Standard; C = Clotrimazole (50 µg).

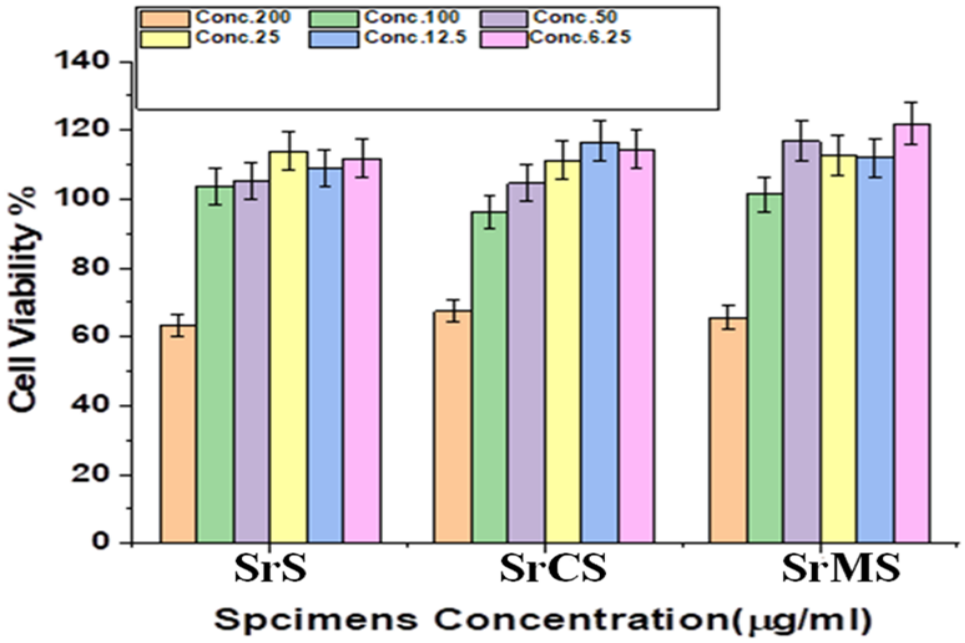

Figure 10 shows the cytocompatibility of the nanoceramic samples against MG-63 cells.

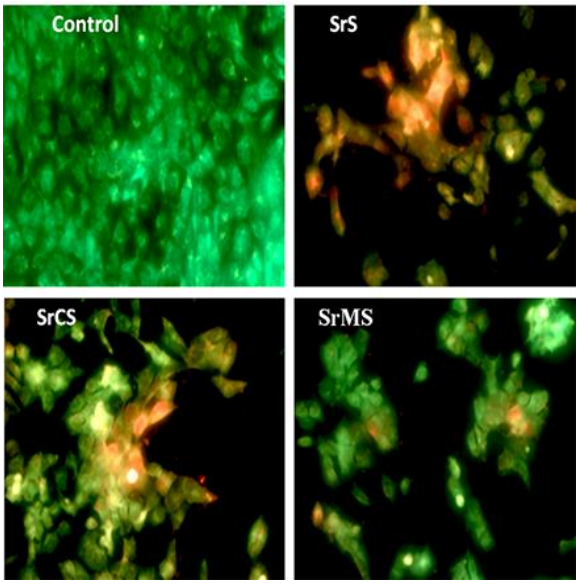

Figure11 captured fluorescence images of SrS, SrCS and SrMS, samples against MG-63 cells.

3.10 Alkaline phosphatase activity

Alkaline phosphatase activity is an early sign of osteoblastic differentiation; therefore, it is utilized as marker of subsequently bone formation. Alkaline phosphatase activity (ALP) for each nanoceramic was .

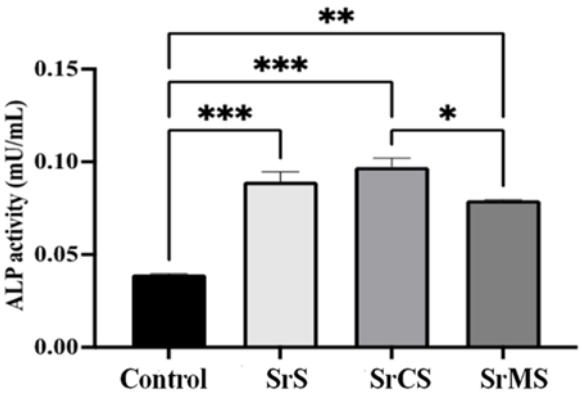

Figure13 ALP activity of SrS, SrCS and SrMS. * p<0.05, ** p< 0.01, *** p<0.001 (n=3).

It was hypothesized this result may be caused by the presence of calcium and silica that induce alkaline phosphatase activity and mineralization through promoting the osteogenesis process of cells as well as Sr which inhibits osteoclastogenesis **[61,62].** Therefore, the ALP results ensure that the fabricated nanoceramics were able to promote the cellular proliferation and differentiation.

Conclusion

carried out at concentration of 100µg/ml against after 24h of exposure to MG-63 cells.

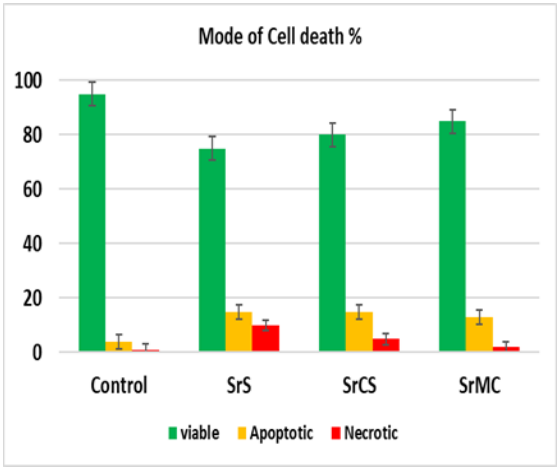

Figure 12 Cell death modes of SrS, SrCS and SrMS samples against MG-63 cells.

Figure 13 show that all nanoceramics have significantly higher ALP activity than the control, confirming osteoid formation and mineralization. However, it is clearly seen that SrCS was able to induce higher ALP activity than other nanoceramics.

In this research, strontium silicate was prepared through the wet method in a water-glass medium, alone or with partial substitution of SrO by either CaO or MgO. Sintering of the samples at 900 °C revealed the crystallization of strontium silicate ($SrSiO_3$), wollastonite ($CaSiO_3$), enstatite ($MgSiO_3$), and cristobalite (SiO_2) in nano size grain microstructure, which is clear in TEM micrographs. The zeta potential confirmed that all the samples carried negative charges. After soaking the samples in SBF, the bioactivity studies illustrated the precipitation of nano size particles of hydroxyapatite on all the samples, which was confirmed through FTIR along with SEM and EDX analyses. Also, compared to other nanoceramics, SrS nanoceramic was found to be more efficient against the tested bacterial strains. All the samples possess substantial cytocompatibility compared to control cells. Alkaline phosphatase activity illustrated that all samples have the potential to induce biomineralization and cellular differentiation. Consequently, the manufactured nanoceramics in this study could be employed as a promising biomaterial for use in bone tissue regeneration.

Author Contribution:
All authors have equally contributed to the following tasks, made co-design of experimental set-up and

conduct of all experiments; generation and preparation of results for publishing; interpretation of results; preparation of original draft; joint preparation of the subsequent drafts. In addition, they have conceptualized the study; funding arrangement; editing and correction of all drafts.

Funding

"This research article was supported by Science, Technology & Innovation Funding Authority (STDF) under grant project number 44846.

References

[1] P.K. Khan, A. Mahato, B. Kundu S.K. Nandi, P. Mukherjee, S. Datta, S. Sarkar, J. Mukherjee, S. Nath, V.K. Balla, C. Mandal, Influence of single and binary doping of strontium and lithium on in vivo biological properties of bioactive glass scaffolds, Scientific Reports 6 (1) (2016) 32964.

[2] J.J. Li, C.R. Dunstan, A. Entezari, Q. Li, R. Steck, S. Saifzadeh, A. Sadeghpour, J.R. Field, A. Akey, M. Vielreicher, O. Friedrich, Novel Bone Substitute with High Bioactivity, Strength, and Porosity for Repairing Large and Load-Bearing Bone Defects, Advanced Healthcare Materials 8 (8) (2019) 1801298.

[3] T.R. Su, T.H. Huang, C.T. Kao, H.Y. Ng, Y.C. Chiu, T.T. Hsu, The calcium channel affect osteogenic differentiation of mesenchymal stem cells on strontium-substituted Calcium silicate/poly-ε-caprolactone scaffold, Processes, 8 (2) (2020) 2227-9717.

[4] J.Y. Reginster, R. Deroisy, I. Jupsin, Strontium ranelate: a new paradigm in the treatment of osteoporosis, Drugs of Today (Barcelona, Spain: 1998) 39 (2) (2003) 89-101.

[5] E. Bonnelye, A. Chabadel, F. Saltel, P. Jurdic, Dual effect of strontium ranelate: stimulation of osteoblast differentiation and inhibition of osteoclast formation and resorption in vitro, Bone 42(1) (2008) 129-138.

[6] A.K. Khalifa, S.A. Diab, G.M. Hashem, E.F. Alalkamy, M.F. Yacoub, New promising avenue for the simvastatin combination with residronate, strontium ranelate and raloxifene in experimentally-induced osteoporosis, The Egyptian Rheumatologist 42 (1) (2020) 63-69.

[7] D.L. Kendler, Strontium ranelate—data on vertebral and nonvertebral fracture efficacy and safety: mechanism of action, Current Osteoporosis Reports 4 (1) (2006) 34-39.

[8] J.Y. Reginster, A. Neuprez, N. Dardenne, C. Beaudart, P. Emonts, O. Bruyere, Efficacy and safety of currently marketed anti-osteoporosis medications, Best Practice & Research Clinical Endocrinology & Metabolism 28 (6) (2014) 809-834.

[9] J. Liu, K. Li, H. Wang, M. Zhu, H. Yan, Rapid formation of hydroxyapatite nanostructures by microwave irradiation, Chemical physics letters 396 (4) (2004) 429-432.

[10] Y. Wang, X. Ren, X. Ma, W. Su, Y. Zhang, X. Sun, X. Li, Alginate-intervened hydrothermal synthesis of hydroxyapatite nanocrystals with nanopores, Crystal Growth & Design 15 (4) (2015) 1949-1956.

[11] R.C. Richard, J. Dai, M.S. Sader, G.A. Soares, R.M.S.M. Thiré, Characterization of β-TCP, β-TCMP and BCMP Produced by Hydrolysis, Bioceramics Development and Applications 2013.

[12] M. Mabrouk, S.M. Mousa, W. A. Abd ElGhany, M.T. Abo-elfadl, G.T. El-Bassyouni, Bioactivity and cell viability of Ag+- and Zr4+-co-doped biphasic calcium phosphate, Applied Physics A 127(12) (2021) 948.

[13] K.Jamuna-Thevi, N.M. Daud, M.A. Kadir, H. Hermawan, The influence of new wet synthesis route on the morphology, crystallinity and thermal stability of multiple ions doped nanoapatite, Ceramics International, 40 (1) (2014) 1001-1012.

[14] M. Pretto, A.L. Costa, E. Landi, A. Tampieri, C. Galassi, Dispersing behavior of hydroxyapatite powders produced by wet- chemical synthesis, Journal of the American Ceramic Society 86 (9) (2003) 1534-1539 .

[15] M. Zhang, W. Zhai, K. Lin, H. Pan, W. Lu, J. Chang, Synthesis, in vitro hydroxyapatite forming ability, and cytocompatibility of strontium silicate powders, Journal of Biomedical Materials Research Part B: Applied Biomaterials 93(1) (2010) 252-257.

[16]R. Jugdaohsingh, Silicon and bone health, The journal of nutrition, health & aging11 (2007).

[17] S. Wang, X. Wang, F.G. Draenert, O. Albert, H.C. Schröder, V. Mailänder, G. Mitov, W.E. Müller, Bioactive and biodegradable silica biomaterial for bone regeneration, Bone 67(2014) 292-304 .

[18] F.E. Imrie, J.M.S. Skakle, I.R. Gibson, Preparation of copper-doped hydroxyapatite with varying x in the composition $Ca_{10}(PO_4)_6Cu_xO_yH_z$, Bioceram Dev Appl S1 2013.

[19] M. Mabrouk, S. A. ElShebiney, S. H. Kenawy, G. T. El-Bassyouni E. M. Hamzawy, Novel, cost-effective, Cu-doped calcium silicate nanoparticles for bone fracture intervention: Inherent bioactivity and in vivo performance, Journal of Biomedical Materials Research Part B: Applied Biomaterials 107 (2) (2019) 388- 399.

[20] M. Mabrouk, S. K. Taha, M. A. Abdel Hamid, S. H. Kenawy, E. A. Hassan, G. T. El-Bassyouni, Radiological evaluations of low cost wollastonite nano-ceramics graft doped with iron oxide in the

treatment of induced defects in canine mandible, Journal of Biomedical Materials Research Part B: Applied Biomaterials 109 (7) (2021) 1029- 1044.

[21] P. Mei, S. Jiang, L. Mao, Y. Zhou, K. Gu, C. Zhang, X. Wang, K. Lin, C. Zhao, M. Zhu, In situ construction of flower-like nanostructured calcium silicate bioceramics for enhancing bone regeneration mediated via FAK/p38 signaling pathway. *Journal of nanobiotechnology 20*(1) (2022) 1-17.

[22] A.E Alecu, G.C. Balaceanu, A.I. Nicoara, I.A. Neacsu, and C. Busuioc, Synthesis and Characterization of Porous Forsterite Ceramics with Prospective Tissue Engineering Applications. *Materials 15*(19) (2022) 6942.

[23] H.A. Abo-Mosallam, E.A. Mahdy, The influence of MgO on the crystallization behaviour and properties of SrO-rich phosphosilicate glasses, Ceramics International 46 (8) (2020) 12009-12014.

[24] S. Wang, L. Liu, X. Zhou, D. Yang, Z.A. Shi, Y. Hao, Effect of strontium-containing on the properties of Mg-doped wollastonite bioceramic scaffolds, Biomedical engineering online 18(1) (2019) 119.

[25] M. Mabrouk, S. H. Kenawy, G. E. El-Bassyouni, A.A.E.I. Soliman, E. M.A. Hamzawy, Cancer cells treated by clusters of copper oxide doped calcium silicate, Adv Pharm Bull 9 (2019).

[26] J.H. Jorgensen, J.D. Turnidge, Susceptibility test methods: dilution and disk diffusion methods, Manual of clinical microbiology (2015) 1253-1273.

[27] M. Elgayyar, F.A. Draughon, D.A. Golden, J.R. Mount, Antimicrobial activity of essential oils from plants against selected pathogenic and saprophytic microorganisms, Journal of food protection, 64 (2001).

[28] S. Kargozar, M. Montazerian, E. Fiume, F. Baino, Multiple and promising applications of strontium (Sr)-containing bioactive glasses in bone tissue engineering, Frontiers in bioengineering and biotechnology 7 (2019).

[29] A. Nilchi, B. Maalek, A. Khanchi, M.G. Maragheh, A. Bagheri, Cerium (IV) molybdate cation exchanger: synthesis, properties and ion separation capabilities. Radiation physics and chemistry 75 (2) (2006) 301-308.

[30] M. Gigantino, D. Kiwic, A. Steinfeld, Thermochemical energy storage via isothermal carbonation-calcination cycles of MgO-stabilized SrO in the range of 1000–1100 ºC, Solar Energy 188 (2019) 720-729.

[31] R. Maddalena, K. Li, P.A. Chater, S. Michalik, A. Hamilton, Direct synthesis of a solid calcium-silicate-hydrate (CSH), Construction and Building Materials 223 (2019) 554-565.

[32] D. Bizari, M. Rabiee, F. Moztarzadeh, M. Tahriri, S.H. Alavi, R. Masaeli, Synthesis, characterization and biological evaluation of sol-gel derived nanomaterial in the ternary system 64% SiO2—31% CaO—5% P2O5 as a bioactive glass: In vitro study, Ceramics–Silikáty, 57 (3) (2013) 201-209.

[33] S. Palakurthy, In vitro evaluation of silver doped wollastonite synthesized from natural waste for biomedical applications, Ceramics International, 45(18) (2019) 25044-25051.

[34] E. Landi, A. Tampieri, G. Celotti, L. Vichi, M. Sandri, Influence of synthesis and sintering parameters on the characteristics of carbonate apatite, Biomaterials 25 (10) (2004) 1763-1770.

[35] S.M. Salman, S.N. Salama, H.A. Abo-Mosallam, Crystallization characteristics and physico-chemical properties of glass–ceramics based on Li2O–ZnO–SiO2 system, Boletín de la Sociedad Española de Cerámica y Vidrio 56(5) (2017) 205-214.

[36] H. Nagasawa, T. Suzuki, M. Ito, M. Morioka, Diffusion in single crystal of melilite: interdiffusion of Al+ Al vs. Mg+ Si, *Physics and Chemistry of Minerals 28* (10) (2001)706-710.

[37] S.J. Liu, Y.F. Zhang, W. He, Y.Z. Yue, Transparent phosphosilicate glasses containing crystals formed during cooling of melts, Journal of non-crystalline solids 357 (24) (2011) 3897-3900.

[38] L.A. Adams, E.R. Essien, E.E. Kaufmann, A new route to sol-gel crystalline wollastonite bioceramic, Journal of Asian Ceramic Societies 6 (2) (2018) 132-138.

[39] G.E.J. Poinern, R.K. Brundavanam, X. Thi Le, P.K. Nicholls, M.A. Cake, D. Fawcett, The synthesis, characterisation and in vivo study of a bioceramic for potential tissue regeneration applications, Scientific Reports 4 (1) (2014) 6235.

[40] T. Perraki, A. Orfanoudaki, Study of raw and thermally treated sepiolite from the Mantoudi area, Euboea, Greece, Journal of Thermal Analysis and Calorimetry 91 (2) (2008) 589-593.

[41] I.P. Sahu, D.P. Bisen, R.K. Tamrakar, K.V.R. Murthy, M. Mohapatra, Luminescence studies on the europium doped strontium metasilicate phosphor prepared by solid state reaction method, Journal of Science: Advanced Materials and Devices 2 (1) (2017) 59-68.

[42] H. Sun, S. He, P. Wu, C. Gao, P. Feng, T. Xiao, Y. Deng, C. Shuai, A novel MgO-CaO-SiO2 system for fabricating bone scaffolds with improved overall performance, Materials 9 (2016) 287.

[43] Y. Zhu, M. Zhu, X. He, J. Zhang, C. Tao, Substitutions of strontium in mesoporous calcium silicate and their physicochemical and biological properties, Acta Biomaterialia 9 (5) (2013) 6723-6731.

[44] M. Saqaei, M. Fathi, H. Edris, V. Mortazavi, Preparation and biocompatibility evaluation of

bioactive glass–forsterite nanocomposite powder for oral bone defects treatment applications, Materials Science and Engineering: C 56 (2015) 409-416.

[45] N. Chandrasekar, K. Kumar, K.S. Balasubramnian, K. Karunamurthy, R. Varadharajan, Facile synthesis of iron oxide, iron cobalt and zero valent iron nanoparticles and evaluation of their ant microbial activity, free radical scavenging activity and antioxidant assay, Digest Journal of Nanomaterials & Biostructures (DJNB) 8 (2013) 765-775.

[46] S.D. Purohit, H. Singh, R. Bhaskar, I. Yadav, C.F. Chou, M.K. Gupta, N.C. Mishra, Gelatin—alginate—cerium oxide nanocomposite scaffold for bone regeneration, Materials Science and Engineering: C 116 (2020) 111111.

[47] H.S. Nanda, Covalent Surface Modification of Cerium Oxide Nanoparticles Promising for Nanomedicine Application 2016.

[48] H.A. Abo-Mosallam, S.N. Salama, S.M. Salman, Formulation and characterization of glass–ceramics based on Na2Ca2Si3O9–Ca5 (PO4) 3F–Mg2SiO4-system in relation to their biological activity, Journal of Materials Science: Materials in Medicine 20 (12) (2009) 2385-2394.

[49] V.K. Vyas, A.S. Kumar, A. Ali, S. Prasad, P. Srivastava, S.P. Mallick, M. Ershad, S.P. Singh, R. Pyare, Assessment of nickel oxide substituted bioactive glass-ceramic on in vitro bioactivity and mechanical properties, Boletín de la sociedadespañola de cerámica y vidrio 55(6) (2016) 228-238.

[50] S.K. Venkatraman, R. Choudhary, N. Vijayakumar, G. Krishnamurithy, H.R.B. Raghavendran, M.R. Murali, T. Kamarul, A. Suresh, J. Abraham, S. Swamiappan, Investigation on bioactivity, mechanical stability, bactericidal activity and in-vitro biocompatibility of magnesium silicates for bone tissue engineering applications, Journal of Materials Research 37 (2) (2022) 608-621.

[51] E. Dietrich, H. Oudadesse, A. Lucas- Girot, M. Mami, In vitro bioactivity of melt- derived glass 46S6 doped with magnesium, Journal of Biomedical Materials Research Part A 88 (4) (2009) 1087-1096

[52] H.G.H. Hammad, A.A. Mostafa, A.M. Hashem, H. Oudadesse, N.A. Badr, S.I. Habib, M. Mabrouk, A.A. Mahmoud, M.I. El-Gohary, Bioactivity and drug delivering ability of a chitosan/46S6 melted bioactive glass biocomposite scaffold, Int Ceram Rev 62 (6) (2013) 444-452.

[53] A.R. Chakhmouradian, E.P. Reguir, R.H. Mitchell, Strontium-apatite: New occurrences, and the extent of Sr-for-Ca substitution in apatite-group minerals, The Canadian Mineralogist 40 (1) (2002) 121-136.

[54] J.S. Fernandes, P. Gentile, R.A. Pires, R.L. Reis, P.V. Hatton, Multifunctional bioactive glass and glass-ceramic biomaterials with antibacterial properties for repair and regeneration of bone tissue, Acta biomaterialia 59 (2017) 2-11.

[55] M.J. Hajipour, K.M. Fromm, A.A. Ashkarran, D.J. de Aberasturi, I.R. de Larramendi, T. Rojo, V. Serpooshan, W.J. Parak, M. Mahmoudi, Antibacterial properties of nanoparticles, Trends in biotechnology 30 (10) (2012) 499-511.

[56] S.Makhluf, R. Dror, Y. Nitzan, Y. Abramovich, R. Jelinek, A. Gedanken, Microwave- assisted synthesis of nanocrystalline MgO and its use as a bacteriocide, Advanced Functional Materials, 15 (10) (2005) 1708-1715.

[57] K. Krishnamoorthy, G. Manivannan, S.J. Kim, K. Jeyasubramanian, M. Premanathan, Antibacterial activity of MgO nanoparticles based on lipid peroxidation by oxygen vacancy, Journal of Nanoparticle Research 14 (9) (2012) 1063.

[58] C.T. Yu, F.M. Wang, Y.T. Liu, A.K.X. Lee, T.L. Lin, Y.W. Chen, Enhanced proliferation and differentiation of human mesenchymal stem cell-laden recycled fish gelatin/strontium substitution calcium silicate 3D scaffolds, Applied Sciences, 10(6) (2020) 2168.

[59] G. Krishnamurithy, S. Mohan, N.A. Yahya, A.Mansor, M.R. Murali, H.R.B.Raghavendran, R.Choudhary, S. Sasikumar,T. Kamarul, The physicochemical and biomechanical profile of forsterite and its osteogenic potential of mesenchymal stromal cells, PloS one 14(3) (2019) e0214212.

[60] B.Gunay, E.Sarıyar, U.Unal, Z.F.Karagonlar,Ö.Sağlam, Upconversion properties of Tm^{3+}-Er^{3+} co-doped layered perovskites and in-vitro cytotoxicity of their exfoliated nanomaterials, Colloids and Surfaces A: Physicochemical and Engineering Aspects612 (2021) 126003.

[61] K. Lin, L. Xia, H. Li, X. Jiang, H. Pan, Y. Xu, W.W.Lu, Z. Zhang, J. Chang, Enhanced osteoporotic bone regeneration by strontium-substituted calcium silicate bioactive ceramics, Biomaterials 34(38) (2013) 10028-10042.

[62] R.D. Prabha, B.P. Nair, N.Ditzel, J.Kjems, P.D. Nair, M. Kassem, Strontium functionalized scaffold for bone tissue engineering, Materials Science and Engineering: C 94 (2019) 509-515.